Journal of Medical Systems (2019) 43: 59
https://doi.org/10.1007/s10916-019-1175-y

IMAGE & SIGNAL PROCESSING

A Comparative Texture Analysis Based on NECT and CECT Images to Differentiate Lung Adenocarcinoma from Squamous Cell Carcinoma

Han Liu[1] · Bin Jing[1] · Wenjuan Han[2] · Zhuqing Long[1] · Xiao Mo[1] · Haiyun Li[1]

Received: 26 September 2018 / Accepted: 21 January 2019 / Published online: 1 February 2019

Abstract

The purpose of the study was to compare the texture based discriminative performances between non-contrast enhanced computed tomography (NECT) and contrast-enhanced computed tomography (CECT) images in differentiating lung adenocarcinoma (ADC) from squamous cell carcinoma (SCC) patients. Eighty-seven lung cancer subjects were enrolled in the study, including pathologically proved 47 ADC patients and 40 SCC patients, and 261 texture features were extracted from the manually delineated region of interests on CECT and NECT images respectively. Fisher score was then used to select the effective discriminative texture features between groups, and the selected texture features were adopted to differentiate ADC from SCC using Support Vector Machine and Leave-one-out cross-validation. Both NECT and CECT images could achieve the same best classification accuracy of 95.4%, and most of the informative features were from the gray-level co-occurrence matrix. In addition, CECT images were found with enhanced texture features compared with NECT images, and combining texture features of CECT and NECT images together could further improve the prediction accuracy. Besides the texture feature, the tumor location information also contributed to the differential diagnosis between ADC and SCC.

Keywords Texture analysis · Lung adenocarcinoma · Squamous cell carcinoma · Non-contrast enhanced computed tomography · Contrast enhanced computed tomography

Introduction

Lung cancer is the leading cause of cancer-related death worldwide [1], and non-small cell lung cancer (NSCLC) accounts for approximately 89% of lung cancers. Adenocarcinoma (ADC) and squamous cell carcinoma (SCC) are two common types of NSCLC, accounting for 45.3% and 23.7% respectively [2]. Recent developments in targeted therapies emphasize the importance of the accurate differential diagnosis between the two subtypes of lung cancer [3, 4]. Currently, the pathological examination based on biopsy or surgical resection is the golden standard for the diagnosis of ADC and SCC, but is mainly limited by the inherently invasive procedures and sampling errors [5, 6]. A non-invasive and effective method is therefore needed to help to make precise diagnoses of ADC and SCC.

Multi-slice CT is a routine and widely used lung cancer examination technique. Compared with non-contrast enhanced computed tomography (NECT) images, contrast enhanced computed tomography (CECT) images are more useful in the clinical evaluation of indeterminate lung nodules because enhancements in malignancies are more obvious than in benign lung nodules [7], leading to an improved image contrast for tumor region. Quantitative morphological assessments of tumor have been the mainstay of oncologic imaging evaluation in clinical practices [8], and in most cases, ADC and SCC patients display similar visual morphological characteristics on both NECT and CECT images, which makes it difficult for the radiologists to directly differentiate each other only by CT images. Therefore, more detailed feature extraction and analysis methods for CT images are definitely

Han Liu and Bin Jing contributed equally to this work.

This article is part of the Topical Collection on *Image & Signal Processing*

✉ Haiyun Li
haiyunli@ccmu.edu.cn

[1] School of Biomedical Engineering, Capital Medical University, Fengtai District, Beijing 100069, China

[2] Department of Radiology, the General Hospital of Chinese People's Armed Police Forces, Beijing 100039, China

required, which may help radiologists and oncologists improve the imaging diagnosis accuracy and better understand the differences between ADC and SCC patients.

Among various image analysis techniques, texture analysis is very useful in detecting subtle tissue changes and could take advantage of the distributional characteristics of gray-levels from medical images to evaluate intra-lesional heterogeneity [9]. It has been effectively used to classify lung nodules with diameters from 2 to 30 mm [10], to make a differential diagnosis between benign and malignant lung nodules [8, 11, 12], and to assess prognosis and treatment response in different oncologic disorders [13–17]. Moreover, previous studies have found that texture features from CT images could reflect the glucose metabolism and stage of NSCLC [18], and were correlated with histopathological markers of angiogenesis and hypoxia in NSCLC [19]. Recently, Wu et al. used the CT texture features from NECT images to discriminate ADC from SCC and achieved the highest area under the curve (AUC) of 0.72 [20]. But till now, no study has been conducted to compare the discriminative performances of multiple texture features derived from the CECT and NECT images in classifying ADC and SCC patients, and it is still unknown whether the CECT images could provide more effective texture features than the NECT images.

In this study, we retrospectively reviewed the ADC and SCC patients with both CECT and NECT images from existed data and designed a texture feature based recognition model to differentiate each other. We would compare the discriminative performances between CECT and NECT images based texture features to explore which imaging method and what texture features would provide better identification of ADC and SCC. Furthermore, we also would like to find out whether combining the texture features of NECT and CECT images together could perform better than single imaging method. Besides texture features, whether the demographic information and tumor characteristics could contribute to the differential diagnosis was also unknown.

Methods

Patients

There were totally 217 patients pathologically diagnosed as ADC or SCC that were reviewed retrospectively, and their image data were obtained from the picture archiving and communication system (PACS) of the General Hospital of Chinese People's Armed Police Forces. All the following inclusion criteria should be fulfilled: 1) Histopathological evidences of ADC or SCC that obtained by tumor resection or biopsy after the CT scans; 2) All patients underwent both NECT and CECT scans respectively; 3) All lesions showed solid-appearing mass and their short axis diameters were at least 10 mm to guarantee region of interests (ROIs) with sufficient area; 4) No patients received any treatments before the CT scan. The exclusion criteria were as follows: 1) The patients who had received any treatments or with the short axis diameter of the lesion less than 10 mm were not enrolled in the study; 2) Three cases in the ADC group showing ground-glass opacities were discarded; 3) Other types of lung cancer identified by histopathology including 4 cases of small cell lung cancer and 1 case of adeno-squamous carcinoma were also discarded. At last, there were 87 patients including 47 ADC patients (age range: 33–85 years, 27 males) and 40 SCC patients (age range: 45–76 years, 35 males) participated in the study.

Image acquisition

All patients were scanned with a 64-slice CT system (Discovery CT750 HD, GE Corporation). NECT and CECT images were respectively acquired encompassing the entire thorax with the same scanning protocol (120 kV; 40–200 mA; scan type: helical; rotation time: 0.6 s; detector coverage: 40 mm; interval: 5 mm; reconstruction width: 1.5 mm; matrix: 512 × 512). CECT scan was performed with 60-s delay after loversol injection (Optiray, Liebel-Flarsheim Canada Inc) through intravenous (dose: 70 ml/person, injection speed: 3 ml/s).

Demographic and tumor characteristics information

The demographic and tumor characteristic features of all ADC and SCC patients are listed in Table 1. Of which, central location represents the tumor arises centrally from main, lobar or segmental bronchi, while peripheral location means the tumor arises from inferior segmental bronchi or alveoli. The differences in patients' gender and tumor location were assessed by the chi-square test, while the differences in patients' age, tumor size, and density were assessed by the independent two-sample T test. The p value<0.05 indicates a significant statistical difference between the two groups.

Texture based recognition model

The whole pipeline of the texture based recognition model was illustrated in Fig. 1, and particularly includes the following three parts: texture features extraction, features selection and SVM-based classification method.

Texture features extraction

The texture features were obtained by MaZda software (Open-source, Version 4.6, http://www.eletel.p.lodz.pl/mazda) [21]. First, 'digital biopsy' method, which was a new paradigm proposed by Sebastian Echegaray et al. [22], was selected to

Table 1 Statistical analysis results of demographic and tumor characteristics

Characteristics	ADC ($n = 47$)	SCC ($n = 40$)	P value
Gender (M/F)	27/20	35/5	0.002
Age	61.0 (35–85)	62.0 (45–76)	0.69
Location (P/C)	35/12	20/20	0.018
Volume	2.79 (0.18–40.42)	5.23 (0.22–23.99)	0.08
Mean CT value on NECT	36.0 (17–57)	35.5 (16–62)	0.67
Mean CT value on CECT	63.0 (36–91)	65.0 (41–85)	0.18

The values in age, volume and mean CT value were displayed with *median* (*range*). The unit for volume is $10^4\ mm^3$, while the unit for CT value is *Hounsfield unit*

Abbreviation: *n* number, *M* male, *F* female, *P* peripheral, *C* central

create ROIs instead of 2D/3D tumor segmentation. We only defined a 2D ROI in one slice of the tumor, and the slice was selected with the maximal cross-sectional area. In this study, we simplified the delineation of ROIs using the paintbrush tool on 2D cross-sections by a radiologist with more than 10 years of experience in thorax diagnosis following the criteria: choosing the mass parenchymal areas, avoiding calcification, necrosis and vacuole. For those tumors involving adhesion with neighboring tissues or accompanying with lobar and segmental atelectasis, the radiologist avoided the inclusion of the adhesive tissues or lung tissue into the ROIs. All of the ROIs were defined on CECT images firstly because tumors display better contour and margin on CECT images than on NECT images, then identical ROIs covering the tumor parenchyma were placed on the same slice of every subject on NECT images, which were illustrated in Fig. 1. Of note, we visually checked the correspondence between the ROIs on CECT images and the tumor regions on NECT images, once the ROI didn't match well, the rigid-body transformation (including translation and rotation) will be used on the ROI to match the tumor locations on NECT images by Mazda software.

After that, five kinds of texture features were calculated including: (1) Histogram, depicting the distribution of pixel values; (2) Gray-level co-occurrence matrix (GLCM), describing the relative relations of pixel pairs along all directions at different distances; (3) Run-length matrix (RLM), reflecting the pixel intensity homogeneity in specific directions; (4) Gradient, measuring the absolute gradient values of 3×3 neighborhoods of pixels; (5) Autoregressive (AR) model, estimating the pixel intensity with four adjacent pixels (left, top, top-left and top-right). In all, 261 features were extracted from each ROI, and detailed definitions of those texture features computed by Mazda could be found in [23, 24].

Feature selection

Considering that not all features will contribute to the between-group classification, the redundant texture features should be discarded. In this study, Fisher Score [25], which

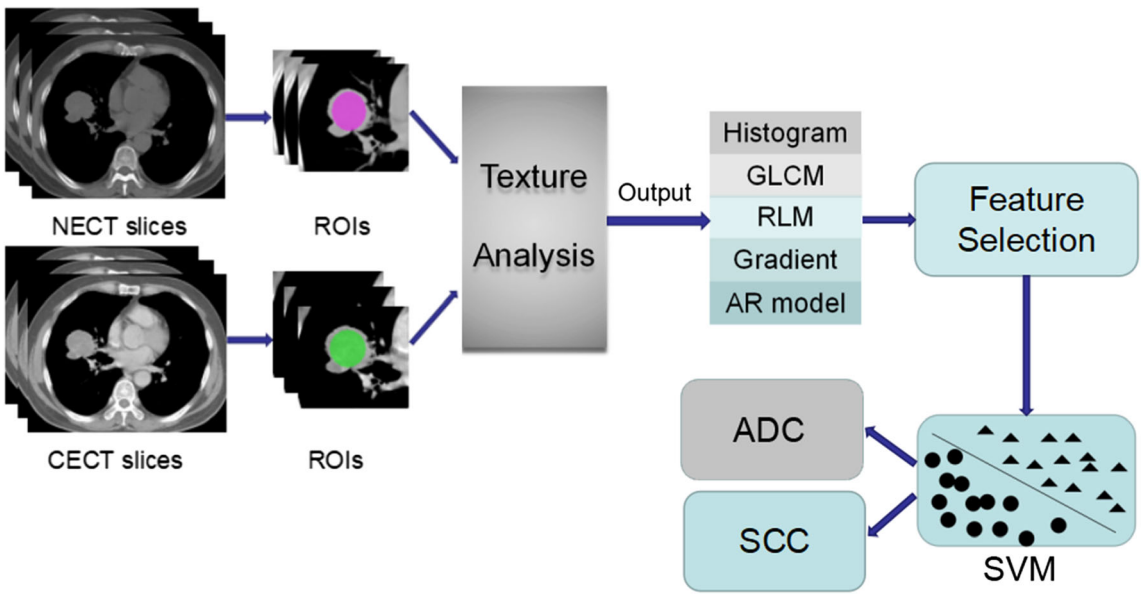

Fig. 1 The texture analysis based model of the classification between ADC and SCC patients

is an effective feature reduction index, was used to sort all features with a descending order based on their importance. For Fisher Score, a high score means a high discriminative power of the feature. It is not easy to determine the optimal threshold for the Fisher Score, so we calculated the accuracy with different numbers of the rearranged features. In order to reduce the computational burden, the feature number was increased with an interval of 5 (i.e. num = 5, 10, 15, 20....260).

SVM-based classification method

Support Vector Machine (SVM) is a widely used machine learning method for classification. Its basic idea is that: the inputting data are non-linearly mapped into a high dimensional feature space where a linear separating hyperplane is created to separate the data [26], and the principle of 'structural risk minimization' is used to find the optimal separating hyperplane with the maximum margin. The detailed algorithm information about SVM could be found in Chang's paper [27].

Before the classification of ADC and SCC, the input features were linearly rescaled from 0 to 1, respectively. Then, radial basis function (RBF), which is defined as $(X, X_i) \rightarrow K(X, X_i) = e^{\gamma |X - X_i|^2}$, was selected as the kernel function, and a grid search method was used to optimize two parameters: γ, width of the RBF, and C, an input parameter for the SVM algorithm, which adjusts the trade-off between having zero training errors and allowing misclassifications. The grid search method is performed with (γ, C) varying along a grid with $\gamma = 2^{-8}, 2^{-7.75}, 2^{-7.5}, \ldots, 2^{8}$ and $C = 2^{-8}, 2^{-7.75}, 2^{-7.5}, \ldots, 2^{8}$, and the ($\gamma$, C) pair with the highest performance was selected as the final model parameters. The classification performance was evaluated with accuracy, sensitivity, and specificity by using the leave-one-out cross-validation (LOOCV).

Recognition performance comparisons

The performances in classifying ADC and SCC patients with the texture features were respectively computed for NECT and CECT images, and the performance using the combined texture features was also calculated. In addition, demographic information and tumor characteristics with significant group differences between ADC and SCC patients were also added to texture feature sets to find out whether they could affect the recognition performance.

Results

The statistical analysis results of patients' demographic and tumor characteristics were illustrated in Table 1. There were significant statistical differences in patients' gender and tumor location: 1) SCC patients had a stronger tendency to occur in males than that in ADC patients; 2) ADC tended to occur in the peripheral lung while there were no obvious location differences in SCC patients; 3) There were no significant statistical differences in patients' age, tumor sizes and density. Two selected examples of ADC and SCC patients with their NECT, CECT images, and hematoxylin-eosin (HE) staining pathological sections were shown in Fig. 2. It was easy to find that there was no obvious visual differences on NECT or CECT images but obvious different cell types and internal structures existed in the pathological manifestation.

The textures features of all subjects were rearranged in descending order by Fisher Score in Fig. 3, which can make an intuitive comparison of the texture features between groups. It should be mentioned that this result was not used in the LOOCV feature selection step, and the main purpose was to display whether the texture features from CECT images were more informative than from NECT images. Interestingly, we can see that texture features of NECT images were more effective before a cross point in Fig. 3 than that of CECT images, but after the cross point, texture features were more informative on CECT images.

After the classification of ADC and SCC using SVM and LOOCV, we achieved three curves of classification accuracy, sensitivity, and specificity with different number of features, which were illustrated in Fig. 4. We could see that a minimum of 5 combined CECT features (S[3,-3]Entropy, S[0,3]SumVarnc, 45dgr_Fraction, S[4,-4]Correlat, S[3,0]DifEntrip) could obtain the best accuracy of 95.4%, while at least 10 combined NECT features (S[2,-2]SumVarncv, Vertl_Fraction, S[2,0]Contrast, S[3,-3]SumOfSqs, S[0,3]SumVarnc, S[2,-2]Entropy, S[0,5]SumAverg, S[5,0]Contrast, S[4,0]InvDfMom, S[2,0]Correlat) were needed to achieve the same accuracy (Fig. 4a), and most of the features were from GLCM except two fraction features which were from RLM. There were 115 features from CECT images and 50 features from NECT images contributed to the high accuracy (≥90%). Most of those features were derived from GLCM, and the others mainly were from RLM (illustrated in Table 2). Meanwhile, combining the texture features of NECT and CECT images could improve the prediction performance (best accuracy: 96.55%). When only using NECT or CECT texture features, combining tumor location information with texture feature sets could also improve the accuracy (best accuracy: 96.55%), but when the texture features of NECT and CECT images have been combined together, adding gender, tumor location or both could not improve the accuracy anymore (best accuracy: 96.55%).

It should be emphasized that the adopted features in the model were just from the training set, and the features may be slightly changed in every fold. We just compared the discriminative powers with the same number of texture features based on CECT and NECT images, but didn't focus on the comparisons using the same texture features. In addition, it

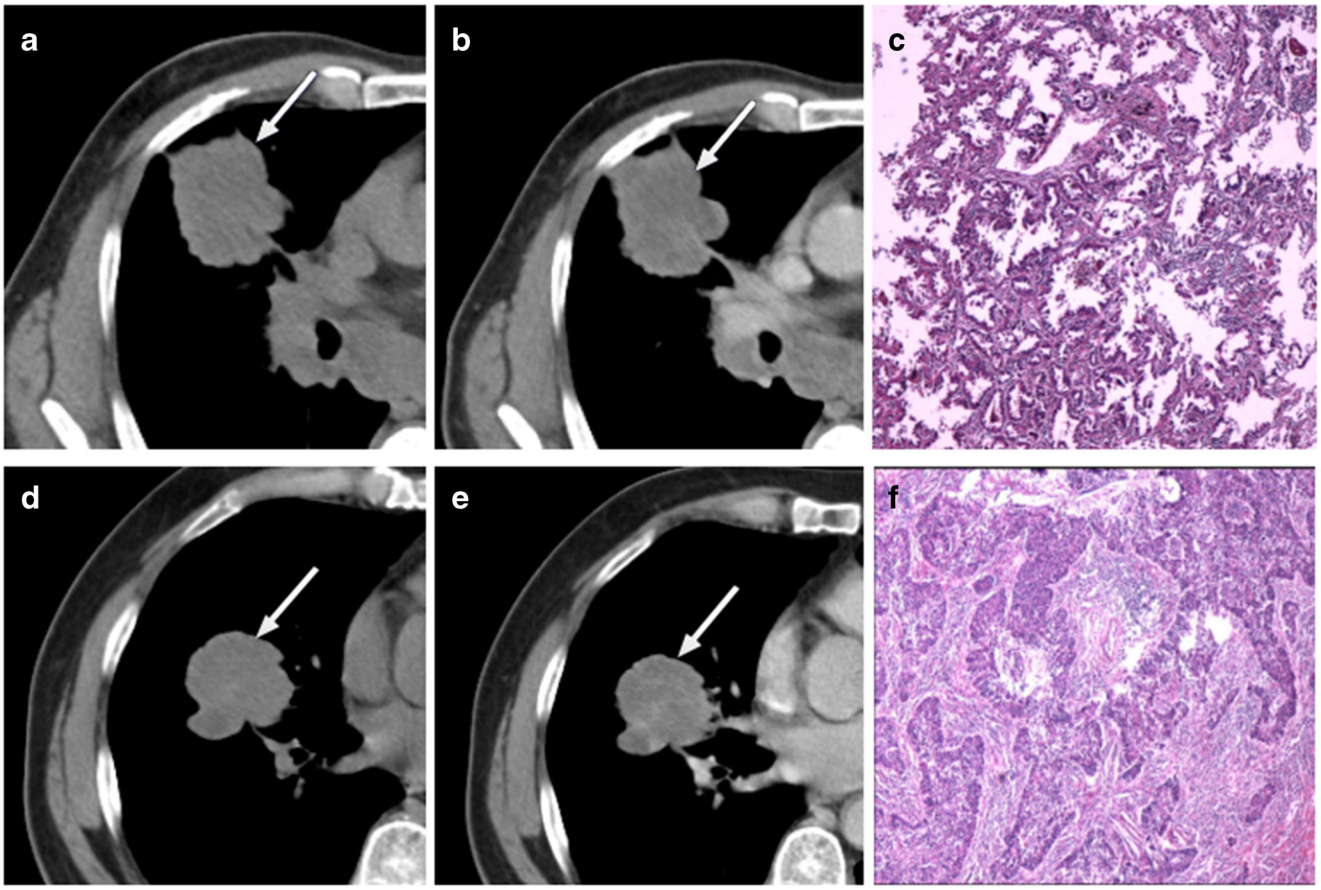

Fig. 2 Two selected examples of ADC and SCC patients with NECT, CECT images and corresponding HE pathological sections. *Figure **a**, **b**, **c** represent the NECT image, CECT image (white arrow) and HE pathological manifestation of one ADC patient respectively. **d**, **e**, **f** represent the NECT image, CECT image (white arrow) and HE pathological manifestation of one SCC patient respectively

could be found in Fig. 4 that the texture features of CECT images showed better specificity than those of NECT images, but differences in the sensitivity between the texture features of NECT and CECT images were not significant (two-sample T test, $P > 0.05$).

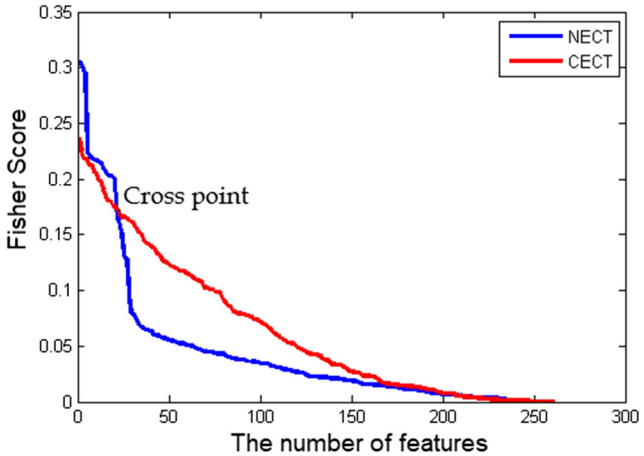

Fig. 3 The sorting results of whole texture features using Feature score. *Of note, the result here was from the whole texture features of the CECT and NECT images and wasn't used in the following LOOCV step

Discussion

We achieved encouraging results in the classification of ADC and SCC patients with the texture based recognition model. The best classification accuracy achieved to 95.4% for NECT and CECT images, and most of the features contribute to the high accuracy were from GLCM. CECT images displayed more informative texture features that contributed to the high recognition accuracy than NECT images, and the specificity of CECT images was also significantly better than NECT images.

One of the great advances in lung cancer diagnosis and treatment in the past decade is personalized medicine, and the therapeutic decisions are based on the specific histologic and genetic characteristics of the tumors [28]. A precise differential diagnosis of ADC and SCC patients is crucial for the appropriate therapeutic decisions. CT texture features were found to be associated with histopathologic features and clinical outcomes in various tumors [29] and were believed to be a rich source of diagnostic information [30–32]. It was difficult to differentiate ADC from SCC patients with the imaging features through visual inspection even by experienced

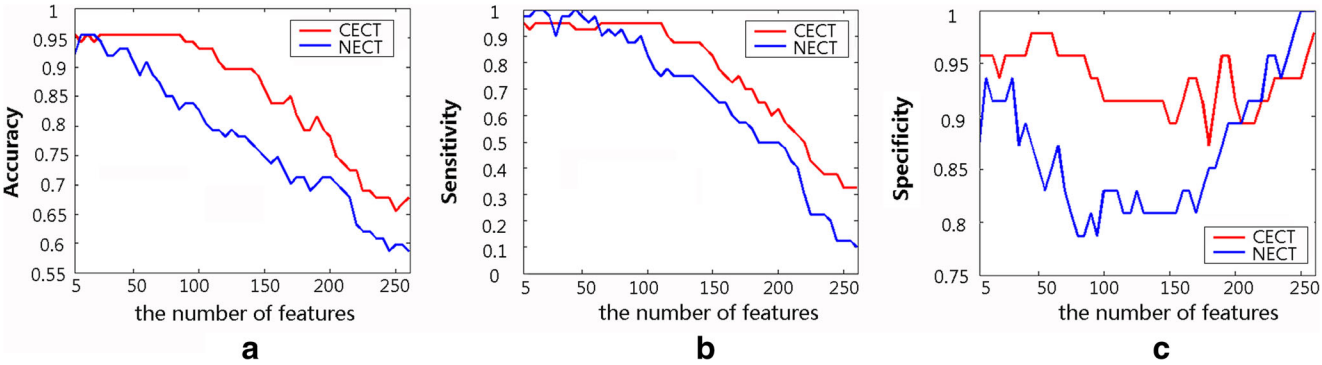

Fig. 4 Results of accuracy, sensitivity, and specificity in the classification of ADC and SCC patients with the proposed method. *Classification performances were obtained with a different number of texture features (interval: 5). Figure **a** The classification accuracy between ADC and SCC; Figure **b** The sensitivity between ADC and SCC; Figure **c**: The specificity between ADC and SCC

radiologists, but the texture based method could make a differential diagnosis with a satisfactory accuracy, which indicated that texture features could detect subtler image information than visual inspection. The texture features had been previously reported to correlate with tumor angiogenesis in NSCLC [19], and our study could further confirm the texture-histopathology correlation. Furthermore, when using only NECT or CECT texture features for discrimination, combining tumor location feature could further improve the accuracy, implying that tumor location is an important marker for the subtype identification of lung cancer.

It is well known that no single texture feature is consistently advantageous, it is reasonable to combine different texture features to improve the texture-based classification accuracy. In this study, GLCM based texture features manifested the best discriminative powers, which were consistent with the study of Vince et al. [33] and may explain why GLCM is the most widely used texture measure. The findings of our study were also similar to a previous study [34], which reported the combined texture features would perform better than the single GLCM-based features in the multiple sclerosis classification.

In our study, although both of CECT and NECT images could get the same best accuracy in the classification of ADC and SCC, CECT images could provide more informative texture features than NECT images, which may be caused by the intensified effect of contrast agent. Therefore, our results could reflect CECT texture features have been enhanced in discriminating ADC and SCC patients than NECT texture features. In another previous study of renal tumors [35], they found the combination of texture features extracted from different CT scanning phases showed dissimilar discriminative powers, and they speculated that this may be associated with the different histologic components and enhancement patterns of the tumors. Inspired by the previous study, the combination of the CECT and NECT texture features was also testified in the study, and the results showed an improved prediction performance, indicating that CECT image could provide some complementary information for the NECT image.

An objective and explicit delineation of ROI is a crucial step in the study. For automatic tumor segmentation, it may be not always workable when some of the tumors show severe adhesion with neighboring tissues in our study. Manual tumor

Table 2 The total extracted texture features and the informative features contributed to high accuracy (≥90%)

Total features ($n = 261$)	Category	The number of informative features	
		ADC vs. SCC (NECT, $n = 50$)	ADC vs. SCC (CECT, $n = 115$)
Histogram ($n = 11$)	Mean, Variance, Skewness, Kurtosis	0	0
GLCM ($n = 220$)	Angular Second Moment, Contrast, Correlation, Sum of Squares, Inverse Difference Moment, Sum Average, Sum Variance, Sum Entropy, Entopy, Difference Variance, Different Entropy	42	106
RLM ($n = 20$)	ShrtREmph, LngREmph, GLevNonUni, RLNonUni, Fraction	8	6
Gradient ($n = 5$)	GrMean, GrVariance, GrSkewness, GrKurtosis, GrNonZeros	0	2
AR model ($n = 5$)	Teta1–4, Sigma	0	1

Abbreviation: *n* number, *GLCM* Gray-level co-occurrence matrix, *RLM* Run-length Matrix, *AR* Autoregressive

selection could precisely delineate the contour of the tumor for every patient, but it is labor-intensity and time-consuming. In addition, the manual ROI could be defined in a 2D or 3D manner, although 3D ROI could provide more texture features, it needs significantly larger computations and more effective feature selection methods, and also may miss the slice-wise heterogeneity information of tumors, which is thought as an important prognostic factor. Taken together, to make the manual delineation simpler, more time-saving and sensitive, we manually delineated 2D ROIs containing the parenchymal parts of the tumor with the largest cross-sectional area and got satisfactory classifying results.

From the viewpoint of differentiation between ADC and SCC, a minimum of 5 combined CECT features could obtain the best accuracy (95.4%), while at least 10 combined NECT features were needed to the same accuracy (See Fig. 4a). Using more CECT or NECT images based texture features could also achieve the identical best accuracy, but no further improvement. Therefore, only a few texture features are needed to ascertain the specific subtype of NSCLC patient. Besides, another not surprising phenomenon was that with the increased number of adopted texture features, the discriminative accuracies declined drastically, especially on NECT images. We speculate this may be related to the redundancy in the texture features, such as the high correlation between features. Wu et al. [20] reported that 75% texture features had absolute pair-wise Pearson correlations higher than 0.8, and 67% were over 0.9, which indicated the importance of the feature selection for the texture analysis study. In our study, Fisher Score was chosen as the feature selection method, and the results demonstrated its effectiveness and feasibility for the texture analysis study.

There are still several limitations in the study: Only one experienced radiologist took part in the delineation of tumor ROIs, more operators may give more reliable ROI segmentation results; The number of the subjects were not large enough, and larger samples should be used to testify the texture based model in the future work.

Conclusion

Both NECT and CECT texture characteristics may act as potential non-invasive markers in discriminating ADC from SCC patients while some texture features have been enhanced on CECT images, and appropriate texture feature selection and combination are vital for the precise discrimination between ADC and SCC patients.

Funding This work was supported by National Natural Science Foundation of China (grant numbers 81220108007), Beijing Natural Science Foundation (No. 4122018). Bin Jing was supported by Beijing Natural Science Foundation (No. 7174282).

Compliance with ethical standards

Conflict of interest The authors declare that they have no conflict of interest.

Ethical approval All procedures performed in studies involving human participants were in accordance with the ethical standards of the national research committee.

Informed consent For this type of study formal consent is not required.

Publisher's Note Springer Nature remains neutral with regard to jurisdictional claims in published maps and institutional affiliations.

References

1. Jemal, A., Siegel, R., Xu, J. et al., Cancer statistics, 2010. *CA Cancer J. Clin.* 60(5):277–300, 2010.
2. Yang, P., Allen, M. S., Aubry, M. C. et al., Clinical features of 5,628 primary lung cancer patients: Experience at Mayo Clinic from 1997 to 2003. *Chest* 128(1):452–462, 2005.
3. Scagliotti, G., Hanna, N., Fossella, F. et al., The differential efficacy of pemetrexed according to NSCLC histology: A review of two phase III studies. *Oncologist* 14(3):253–263, 2009.
4. Shroff, G. S., Benveniste, M. F., de Groot, P. M. et al., Targeted therapy and imaging findings. *J. Thorac. Imaging* 32(5):313–322, 2017.
5. Yano, M., Yoshida, J., Koike, T. et al., The outcomes of a limited resection for non-small cell lung cancer based on differences in pathology. *World J. Surg.* 40(11):2688–2697, 2016.
6. Thunnissen, E., Noguchi, M., Aisner, S. et al., Reproducibility of histopathological diagnosis in poorly differentiated NSCLC: An international multiobserver study. *J. Thorac. Oncol.* 10(1):1354–1362, 2015.
7. Swensen, S. J., Viggiano, R. W., Midthun, D. E. et al., Lung nodule enhancement at CT: Multicenter study. *Radiology* 214(1):73–80, 2000.
8. Dilger, S. K., Uthoff, J., Judisch, A. et al., Improved pulmonary nodule classification utilizing quantitative lung parenchyma features. *J. Med. Imaging* 2(4):041004, 2015.
9. Davnall, F., Yip, C. S., Ljungqvist, G. et al., Assessment of tumor heterogeneity: An emerging imaging tool for clinical practice? *Insights Imaging.* 3(6):573–589, 2012.
10. Orozco, H. M., OOV, V., VGC, S. et al., Automated system for lung nodules classification based on wavelet feature descriptor and support vector machine. *Biomed. Eng. Online* 14(1):1–20, 2015.
11. Dennie, C., Thornhill, R., Sethivirmani, V. et al., Role of quantitative computed tomography texture analysis in the differentiation of primary lung cancer and granulomatous nodules. *Quant. Imaging Med. Surg.* 6(1):6–15, 2016.
12. Hwang, I. P., Park, C. M., Park, S. J. et al., Persistent pure ground-glass nodules larger than 5 mm: Differentiation of invasive pulmonary adenocarcinomas from preinvasive lesions or minimally invasive adenocarcinomas using texture analysis. *Investig. Radiol.* 50(11):798–804, 2015.
13. Ganeshan, B., Panayiotou, E., Burnand, K. et al., Tumour heterogeneity in non-small cell lung carcinoma assessed by CT texture analysis: A potential marker of survival. *Eur. Radiol.* 22(4):796–802, 2012.
14. Giganti, F., Marra, P., Ambrosi, A. et al., Pre-treatment MDCT-based texture analysis for therapy response prediction in gastric

cancer: Comparison with tumour regression grade at final histology. *Eur. J. Radiol.* 90:129–137, 2017.
15. Haider, M. A., Vosough, A., Khalvati, F. et al., CT texture analysis: A potential tool for prediction of survival in patients with metastatic clear cell carcinoma treated with sunitinib. *Cancer Imaging* 17(1):4, 2017.
16. Fried, D. V., Tucker, S. L., Zhou, S. et al., Prognostic value and reproducibility of pretreatment CT texture features in stage III non-small cell lung cancer. *Int. J. Radiat. Oncol. Biol. Phys.* 90(4):834–842, 2014.
17. Emaminejad, N., Qian, W., Kang, Y. et al., Exploring new quantitative CT image features to improve assessment of lung cancer prognosis. In: SPIE Medical Imaging, 2015, 94141M.
18. Balaji, G., Sandra, A., RCD, Y. et al., Texture analysis of non-small cell lung cancer on unenhanced computed tomography: Initial evidence for a relationship with tumour glucose metabolism and stage. *Cancer Imaging* 10(1):137–143, 2010.
19. Ganeshan, B., Goh, V., Mandeville, H. C. et al., Non-small cell lung cancer: Histopathologic correlates for texture parameters at CT. *Radiology* 266(1):326–336, 2013.
20. Wu, W., Chintan, P., Patrick, G. et al., Exploratory study to identify radiomics classifiers for lung cancer histology. *Front. Oncol.* 6(Suppl 2):71, 2016.
21. Materka, A., and Klepaczko, A., MaZda-A software package for image texture analysis. *Comput. Methods Prog. Biomed.* 94(1):66–76, 2009.
22. Echegaray, S., Nair, V., Kadoch, M. et al., A rapid segmentation-insensitive "digital biopsy" method for Radiomic feature extraction: Method and pilot study using CT images of non-small cell lung cancer. *Tomography.* 2(4):283–294, 2016.
23. Haralick, R. M., Shanmugam, K., and Dinstein, I., Textural features for image classification. *IEEE Trans. Syst. Man Cybern.* smc. 3(6): 610–621, 1973.
24. Szczypiński, P. M., Strzelecki, M., Materka, A. et al., MaZda – the software package for textural analysis of biomedical images. Berlin: Springer, 2009, 73–84.
25. Duda, R. O., Hart, P. E., and Stork, D. G., Pattern classification. 2nd edition, Wiley, New York, 2001.
26. Mourão-Miranda, J., Bokde, A. L., Born, C. et al., Classifying brain states and determining the discriminating activation patterns: Support vector machine on functional MRI data. *NeuroImage* 28(4):980–995, 2005.
27. Chang, C. C., and Lin, C. J., LIBSVM: A library for support vector machines. *ACM Trans. Intell. Syst. Technol.* 2(3):1–27, 2011.
28. Travis, W. D., Brambilla, E., Nicholson, A. G. et al., The 2015 World Health Organization classification of lung tumors: Impact of genetic, clinical and radiologic advances since the 2004 classification. *J. Thorac. Oncol.* 10(9):1243–1260, 2015.
29. Lubner, M. G., Smith, A. D., Sandrasegaran, K. et al., CT texture analysis: Definitions, applications, biologic correlates, and challenges. *Radiographics A Review Publication of the Radiological Society of North America Inc*. 37(5):1483, 2017.
30. Aerts, H. J., Velazquez, E. R., Leijenaar, R. T. et al., Decoding tumour phenotype by noninvasive imaging using a quantitative radiomics approach. *Nat. Commun.* 5:4006, 2014.
31. Gillies, R. J., Kinahan, P. E., and Hricak, H., Radiomics: Images are more than pictures, they are data. *Radiology* 278(2):563–577, 2016.
32. Phillips, L., Ajaz, M., Ezhil, V. et al., Clinical applications of textural analysis in non-small cell lung cancer. *Br. J. Radiol.* 91: 20170267, 2017.
33. Vince, D. G., Dixon, K. J., Cothren, R. M. et al., Comparison of texture analysis methods for the characterization of coronary plaques in intravascular ultrasound images. *Comput. Med. Imaging Graph.* 24(4):221–229, 2000.
34. Zhang, J., Tong, L., Wang, L. et al., Texture analysis of multiple sclerosis: A comparative study. *Magn. Reson. Imaging* 26(8):1160–1166, 2008.
35. Yan, L., Liu, Z., Wang, G. et al., Angiomyolipoma with minimal fat: Differentiation from clear cell renal cell carcinoma and papillary renal cell carcinoma by texture analysis on CT images. *Acad. Radiol.* 22(9):1115–1121, 2015.